10-2020

VolKilau: Volcano rapid response balloon campaign during the 2018 Kilauea eruption

Jean Paul Vernier

Lars E. Kalnajs

Jorge Andrés Diaz

Tom Reese

Ernesto Corrales

See next page for additional authors

Recommended Citation

Vernier, Jean Paul; Kalnajs, Lars E.; Diaz, Jorge Andrés; Reese, Tom; Corrales, Ernesto; Alan, Alfredo; Vernier, Hazel; and et al, VolKilau: Volcano rapid response balloon campaign during the 2018 Kilauea eruption (2020). *Bulletin of the American Meteorological Society*, 101(10), E1602-E1618. doi:10.1175/BAMS-D-19-0011.1

BAMS Article

VolKilau

Volcano Rapid Response Balloon Campaign during the 2018 Kilauea Eruption

J.-P. Vernier, L. Kalnajs, J. A. Diaz, T. Reese, E. Corrales, A. Alan, H. Vernier, L. Holland, A. Patel, N. Rastogi, F. Wienhold, S. Carn, N. Krotkov, and J. Murray

ABSTRACT: After nearly 35 years of stable activity, the Kilauea volcanic system in Hawaii went through sudden changes in May 2018 with the emergence of 20 volcanic fissures along the Lower Eastern Rift Zone (LERZ), destroying 700 homes in Leilani Estates and forcing more than 2,000 people to evacuate. Elevated volcanic emissions lasted for several months between May and September 2018, leading to low visibility and poor air quality in Hawaii and across the western Pacific. The NASA-funded VolKilau mission was rapidly mounted and conducted between 11 and 18 June 2018 to (i) profile volcanic emissions with SO_2 and aerosol measurements, (ii) validate satellite observations, and (iii) increase readiness for the next large volcanic eruption. Through a series of balloon-borne measurements with tethered and free-released launches, we measured SO_2 concentration, aerosol concentration, and optical properties 60–80 km downwind from the volcanic fissures using gas sensors, optical particle counters, backscatter sondes, and an aerosol impactor. While most of the measurements made during the Kilauea eruption were ground based, the VolKilau mission represented a unique opportunity to characterize plume properties, constrain emission profiles, study early chemistry involving the conversion of SO_2 into sulfuric acid, and understand the influence of water clouds in the removal of SO_2. This unprecedented combination of measurements has significantly improved our team's ability to assess the atmospheric and human impacts of a major event such as this.

https://doi.org/10.1175/BAMS-D-19-0011.1
Corresponding author: Jean-Paul Vernier, jeanpaul.vernier@nasa.gov
In final form 2 March 2020

AFFILIATIONS: **Vernier**—National Institute of Aerospace, and NASA Langley Research Center, Hampton, Virginia; **Kalnajs and Reese**—Laboratory for Atmospheric and Space Physics, University of Colorado Boulder, Boulder, Colorado; **Diaz, Corrales, and Alan**—GasLab, CICANUM, Universidad de Costa Rica, San Jose, Costa Rica; **Vernier**—Virginia Institute of Marine Science, Gloucester Point, Virginia; **Holland**—University of Hawai'i at Mānoa, Honolulu, Hawaii; **Patel and Rastogi**—Physical Research Laboratory, Ahmedabad, India; **Wienhold**—Swiss Federal Institute of Technology, Zurich, Switzerland; **Carn**—Michigan Technological University, Houghton, Michigan; **Krotkov**—NASA Goddard Space Flight Center, Greenbelt, Maryland; **Murray**—NASA Langley Research Center, Hampton, Virginia

Volcanic eruptions have shaped life on Earth through a combination of geologic and atmospheric impacts. A major eruption can cool the climate system for several years (Robock 2000) from the veil of aerosols produced in the stratosphere (McCormick et al. 1995) that reduces the amount of solar radiation reaching the surface. Tropospheric effusive eruption can strongly deteriorate air quality with the release of sulfur-bearing gas and aerosols (Hansell and Oppenheimer 2004; Hansell et al. 2006) and can potentially affect the 450 million people worldwide living in proximity to volcanoes (Small and Naumann 2001). The Laki eruption in 1783–84 led to an increase of mortality in Iceland by >20% and caused devastating impacts on air quality and crop production throughout Europe (Grattan et al. 2003; Witham and Oppenheimer 2004). Cardiorespiratory and other acute health effects have been observed in the people of Hawaii from the recent eruptions of Kilauea (Longo 2013). Improving the forecast system's information on dangerous, life-threatening volcanic gases and particulate matter (PM) is key to limit local population exposure. The complex physico-chemical processes involved in the evolution of volcanic plumes from the few seconds after their emissions start are not well understood. Observations of sulfate aerosols near volcanic sources (Mather et al. 2003; Kroll et al. 2015) suggest rapid SO_2 oxidation and/or the production of sulfate itself in the magma (Mather et al. 2003). Roberts et al. (2019) recently showed through kinetic-based simulations that high-temperature chemistry quickly forms oxidants such as OH, HO_2, and H_2O_2 that can lead to the production of sulfate within a few seconds after the emission of SO_2 begins. The aqueous pathways for sulfate formation have been studied with photochemical models including isotope markers showing that transition metal ion (TMI) O_2 could indeed dominate the formation of sulfate (Galeazzo et al. 2018) relative to other pathways through H_2O_2 and O_3, which can be rapidly titrated at low pH. In addition, the production of sulfate through new particle formation has been shown to be more frequent under the influence of volcanic emissions compared to background level conditions (Rose et al. 2019; Boulon et al. 2011; Sahyoun et al. 2019). Finally, halogen chemistry leading to ozone depletion has been observed in volcanic plumes (Surl et al. 2015) that could affect oxidation processes. Therefore, measurements in fresh and aged volcanic plumes are extremely important to understand the different pathways of SO_2 oxidation from OH in gas phase and/or H_2O_2, O_3, and O_2 in liquid phase (Galeazzo et al. 2018).

Balloon-based measurements in fresh volcanic plumes are very limited but can provide essential information on the vertical extension of SO_2 and aerosol concentration when the plumes are lofted above the ground due to increased buoyancy. Pieri et al. (2013) reported one of the first blimp- and tethered-balloon-coincident observations of SO_2 and aerosol concentration at the Turrialba Volcano in Costa Rica to validate satellite observations from the Advanced Spaceborne Thermal Emission and Reflection Radiometer (ASTER). Balloon-borne measurements during the Holuhraun eruption in Iceland (Vignelles et al. 2016) provided one of the first aerosol size distribution of volcanic aerosols in very fresh lofted (age ~15 min) plume.

More Recently, NASA Langley Research Center (LaRC) scientists teamed up with researchers from the University of Colorado Boulder and the University of Costa Rica to rapidly deploy gas–aerosol–instrumented balloons during the Volcano Rapid Response Balloon Campaign

during the Kilauea Eruption (VolKilau). Through a series of eight balloon flights in Hawaii between 11 and 18 June 2018, we measured the atmospheric composition in the outflow plumes from the volcanic fissures and from the Halema‘uma‘u main crater.

The purpose of this paper is to describe the preparation, deployment, and preliminary results obtained during VolKilau. With SO_2 and aerosol measurements, we characterized the Kilauea volcanic plumes with high-vertical-resolution balloon data. We show how our measurements can be used to validate satellite observations and model dispersions and to help shed light on microphysical plume evolution.

The 2018 Kilauea eruption

Sudden geological changes of the Kilauea volcanic system. The state of Hawaii forms a chain of islands created over the last 60 million years through the connection of a hot spot transporting magma from the inner mantle. Hawaii is the youngest island in the archipelago and Kilauea is the most recent volcano, having started to erupt 800,000 years ago. After nearly 35 years of stable activity, in May 2018, the Kilauea volcano eruption pattern changed. This produced 20 new fissures and sent lava flowing over streets and neighborhoods (Neal et al. 2019). After wiping out 700 homes and displacing more than 2,000 people, no U.S. eruption was as disruptive since Mount Saint Helens sent ash high into the stratosphere in 1980. The 2018 Kilauea eruption also marked profound changes of the volcanic system with the collapse of the Pu‘u ‘Ō‘ō crater, the draining of the lava lake of the Halema‘uma‘u crater, also called the Kilauea summit, and the emergence of volcanic fissures along the Lower Eastern Rift Zone (LERZ; Fig. 1). Following a 6.9-magnitude earthquake, volcanic fissures opened in the Leilani Estates area on 3 May. More than 20 fissures were reported in the following weeks. The U.S. Geological Survey monitored the extension of the lava fields through thermal infrared cameras mounted on helicopters (Neal et al. 2019). In addition, NASA flew its Gulfstream III jet aircraft to assess the volume of lava extruded from the volcanic fissures with a synthetic aperture radar system from the Jet Propulsion Laboratory. Aside from lava destruction, volcanic fissures continuously emitted 30–60 kt day^{-1} of sulfur dioxide (SO_2) into the atmosphere, which turned into sulfuric acid droplets and formed volcanic fog (vog). This was especially pronounced on the southwestern side of the island and extended out over the western Pacific.

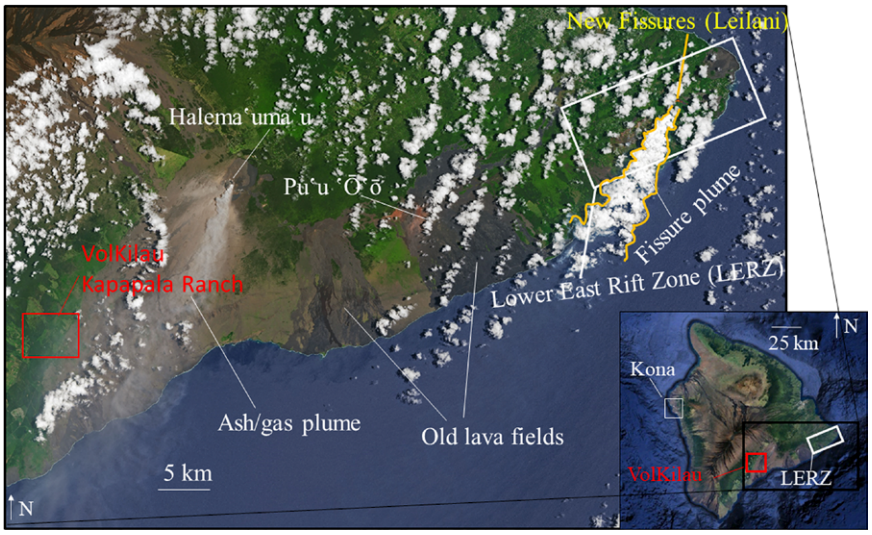

Fig. 1. True-color image from the NASA–USGS *Landsat 8* Operational Land Imager on 14 May 2018 in southern Hawaii. The Pu‘u ‘Ō‘ō crater, Halema‘uma‘u summit, LERZ, and the location of the VolKilau campaign at the Kapapala Ranch are shown.

SO_2 emissions during the Kilauea eruption. The first of the 20 volcanic fissures from the 2018 outbreak was observed on 3 May in the Leilani Estates area, with levels of SO_2 threatening air quality safety in excess of the 1-h primary standard of 75 ppb established by the U.S. Environmental Protection Agency (www.epa.gov/so2-pollution/primary-national-ambient-air

-quality-standard-naaqs-sulfur-dioxide). SO_2 emitted from the Kilauea summit and the LERZ have been measured daily by the Ozone Mapping and Profiling Suite (OMPS). The OMPS nadir mapper is a hyperspectral ultraviolet spectrometer (Flynn et al. 2014; Seftor et al. 2014) on board the NOAA–NASA *Suomi National Polar-Orbiting Partnership* (*SNPP*) satellite measuring SO_2 total vertical column density in Dobson units (1 DU = 2.69×10^{16} SO_2 molecules per cm^2) using a principal component analysis (PCA) algorithm (Zhang et al. 2017; Li et al. 2017). An assumed SO_2 profile shape, represented by its center of mass altitude (CMA) near 2.5 km, was used to derive the lower-tropospheric SO_2 map shown in Fig. 2 (top; Ialongo et al. 2015). Figure 2 (bottom) shows a time series of total daily mass of SO_2 (kilotons; kt) between June and September 2018 (daily OMPS SO_2 maps and tonnages are available online at https://so2.gsfc.nasa.gov/pix/daily/0718/hawaii_0718p.html). The Kilauea eruption lasted for 4 months between May and August 2018 (Fig. 2), with a maximum of 60 kt of SO_2 emitted on 15 June as inferred from OMPS. We note that this estimate could be underestimated due to several factors such as the retrieval algorithm, instrument resolution, and the presence of clouds. The SO_2 plumes were transported by trade winds and affected air quality across Hawaii and the western Pacific (Fig. 2, bottom).

During the 2018 eruption at Kilauea's LERZ, the USGS reported SO_2 emissions over 30 kt day^{-1}, a value that could be influenced by instrument saturation and wind speed assumptions (www.usgs.gov/faqs/how-much-sulfur-dioxide-so2-gas-does-k-lauea-emit?qt-news_science_products=0#qt-news_science_products). Figure 3 shows steam and gas emitted by the volcanic cone produced by Fissure 8. The subsequent transformation of SO_2 into sulfate aerosols forms vog, which is observed in a photo taken 20 km north of Kona on 10 June. The large extension of the vog is also evident in the true color image on 7 June, from the Visible Infrared Imaging Radiometer Suite (VIIRS) on the *SNPP* satellite, characterized by a gray-blueish veil observed hundreds of miles downwind from Hawaii (Fig. 3). While the impacts of the Kilauea eruption on aviation were minimal, the vog presented a serious threat to air quality across the island and largely affected the tourist industry (Neal et al. 2019).

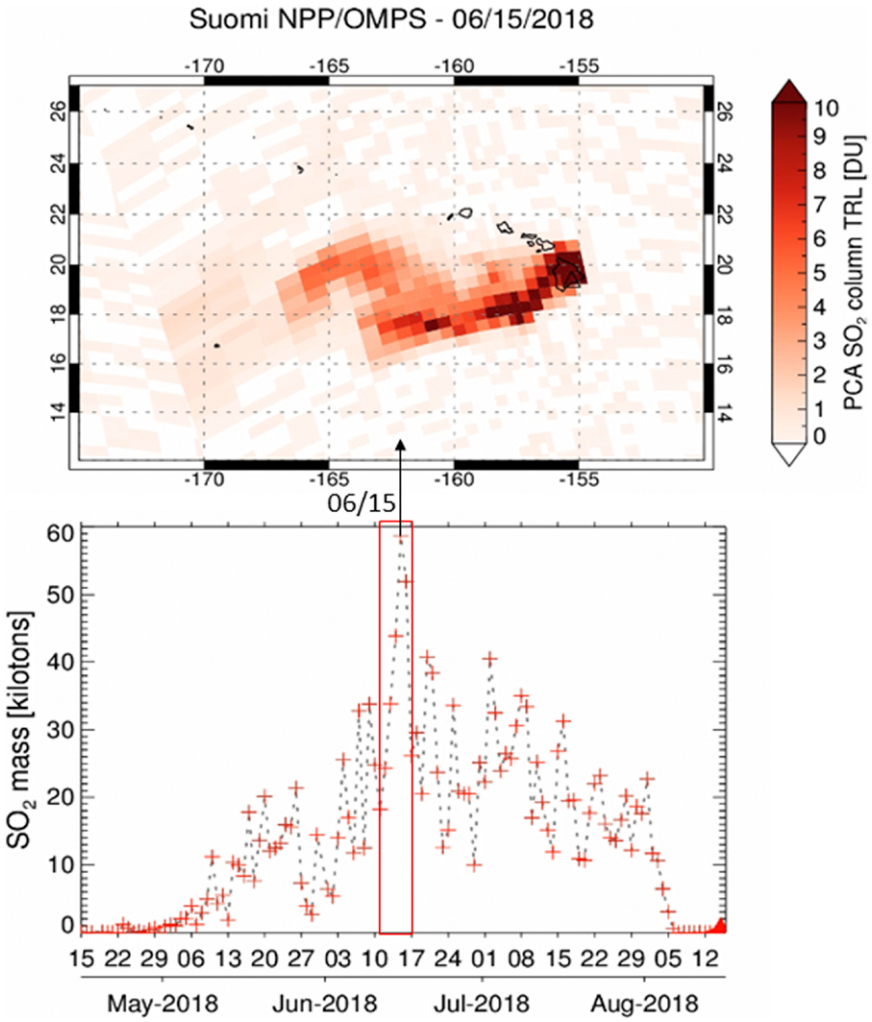

Fig. 2. (bottom) Time series of daily SO_2 mass (kilotons) from OMPS/*SNPP* nadir mapper during the 2018 Kilauea eruption and (top) map of lower-tropospheric SO_2 on 15 Jun 2018 using the PCA algorithm.

Campaign preparation and planning

Volcanic eruptions are by nature challenging to study. Being quasi-unpredictable and

sudden, scientists often rely on satellite observations to assess their atmospheric impacts. Extreme conditions associated with volcanic eruptions can make field measurements dangerous and thus rare. Finally, the composition of volcanic emissions, their dependency on geological processes, and the different stages of plume physico-chemical processing when entering the atmosphere result in complex atmospheric impacts. Heat buoyancy created near volcanic sources generates a plume aloft that cannot always be captured by ground-based measurements, enhancing the value of airborne instruments.

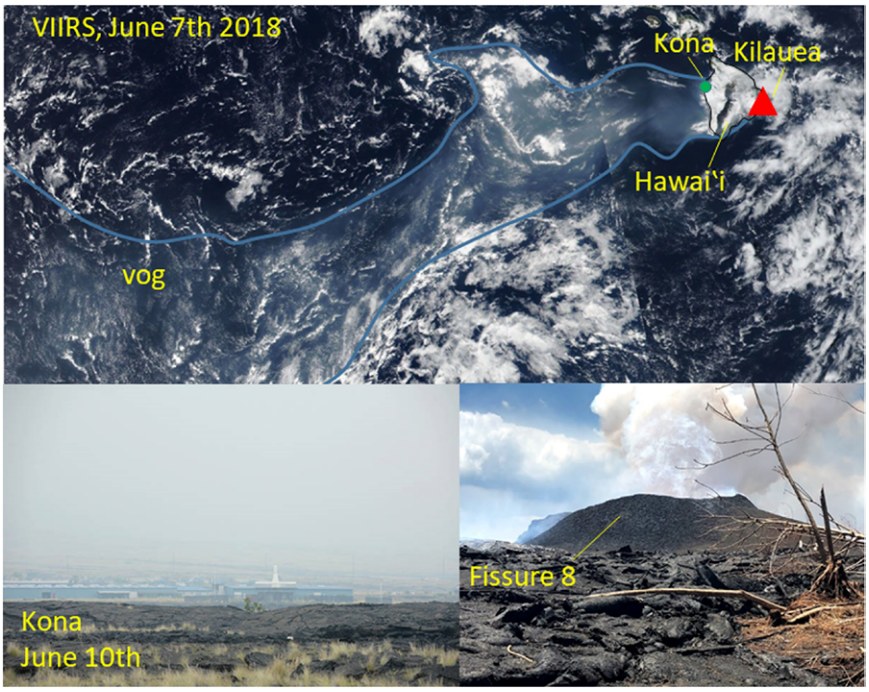

Fig. 3. (top) True-color image showing the vog across the western Pacific observed by VIIRS/*SNPP* on 7 Jun 2019. (bottom) Photos of (left) the vog in Kona on 10 Jun and (right) volcanic emissions from Fissure 8 on 18 Jun.

Our team is affiliated with the NASA Applied Sciences Disasters program (https://disasters.nasa.gov/kilauea-hawaii-eruption-2018) and the Volcano Response (VolRes) international initiative to deploy during and after volcanic eruptions. Within 15 days, VolKilau was on the ground in Hawaii, nearly 60 km downwind from fissures and 20 km from the Halema‘uma‘u crater, to study SO_2 and aerosol emissions from the Kilauea eruption. We deployed a variety of balloon measurement payloads downwind from the eruptive vents to profile SO_2 and aerosol concentrations in the plume, improve model simulations, and validate satellite observations of SO_2 and aerosols. We used forecast maps of SO_2 provided by the University of Hawai‘i at Mānoa (Businger et al. 2015) to choose a deployment location and sample the outflows of Kilauea emission zones. The NOAA Hybrid Single-Particle Lagrangian Integrated Trajectory (HYSPLIT) model (Draxler and Hess 1997; Stein et al. 2015) was initialized between 50 and 700 m above the local terrain to account for buoyancy created at the emission sources. The volcanic plumes originated from three different locations (Fissure 8 in the LERZ, Pu‘u ‘Ō‘ō crater, and Halema‘uma‘u crater). Fissure 8 became the largest source of SO_2, with fluxes between 30 and 60 kt day^{-1} a few weeks after the beginning of the fissure outbreak forming a volcanic cone (photo, Fig. 3). The Pu‘u ‘Ō‘ō crater, which rapidly collapsed after the new fissures started erupting, became a minor source. However, the Kilauea summit also occasionally produced ash clouds up to 10,000 ft (~3 km) and was an additional relatively small source of SO_2 compared to Fissure 8.

After exploring several options remotely, it became clear that choosing a location near the Leilani Estates area could be dangerous given the potential high levels of SO_2 measured on the ground in proximity of the fissures, and became further complicated when the area was restricted to only emergency responders and local residents. The best option would become to deploy downwind from Fissure 8, where trade winds were pushing volcanic emissions toward us at acceptable concentrations for outdoor activities. The Kapapala Ranch (19.263°N, 155.445°W), located along Highway 11 between the Kapapala Forest Reserve and the Hawaii Volcanoes National Park, thus became a viable option, especially given past deployment experience of the team.

The VolKilau campaign

Concept. The VolKilau campaign was designed to study the atmospheric outflow from the Kilauea volcanic emissions with gas and aerosol measurements. The objectives of this mission were to (i) profile volcanic emissions, (ii) validate satellite observations, and (iii) be prepared for the next major volcanic eruption. The first and second objectives relied on obtaining vertically-resolved data of SO_2 and aerosols through the atmosphere. VolKilau was based on three types of balloon operations (Fig. 4): 1) tethered-balloon activities to sample the volcanic plume below 2 km, 2) low-level cut-down balloon flight to optimize the measurements in the plume and terminate the flight early for recovery, and 3) free-released balloons to sample volcanic outflows from the fissures and also high-altitude ash clouds injected occasionally from the Kilauea summit.

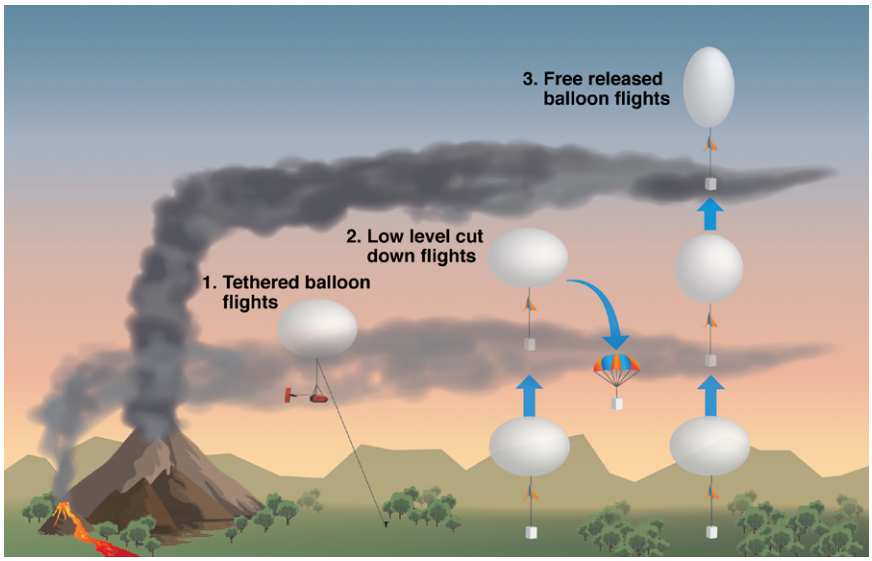

Fig. 4. Balloon activities during the VolKilau campaign to sample volcanic plumes emitted at low altitudes from the fissures in the LERZ and at higher levels from explosive events at the Kilauea summit.

Payloads. The payloads selected for the campaign measure SO_2 and aerosol optical, physical, and chemical properties. They include the following.

ROPC. The Laboratory of Atmospheric and Space Physics (LASP) lightweight OPC (ROPC) is a lightweight and low-cost balloon-borne optical particle counter (OPC), based on a commercially available optical head (Met One 9722) integrated with a flow control system and radiosonde telemetry system. This is the smallest of the balloon-borne OPCs developed at LASP and is well suited to measurements in the troposphere with relatively high aerosol loadings. The size range in radius is between 0.15 and 5 μm, with number concentration ranging from 1 to 3×10^5 L^{-1} in six size bins. The ROPC reaches a coincident counting threshold near 3×10^5 L^{-1}. Above this limit, there is a statistically significant probability that more than one particle may pass through the laser beam at one time, leading to an undercounting of particles. While the instrument will still respond to particle concentrations above the coincidence threshold, the measurement becomes qualitative in nature due to the increasing probability of coincident particles. Mather et al. (2003, 2012) reported sulfate size distributions in the plumes of the Kilauea and Masaya Volcanos with peaks near 0.15-μm radius. Thus, our OPC measurements do not fully capture the entire size distribution of sulfate and therefore are likely provide lower limit estimates of total aerosol number concentration.

LOPC. The Langley Optical Particle Counter (LOPC) is another lightweight OPC developed at NASA LaRC and adapted for weather balloon flight applications, also using the Met One 9722 particle counter with a small external pump from Particle Plus, Inc. The data logging is based on Raspberry Pi and is compatible with an iMet meteorological radiosonde. The OPC includes eight channels with sizes between 0.15 and 10 μm, and the measurement range is similar to the ROPC.

COBALD. The Compact Optical Backscatter and Aerosol Detector (COBALD) is a lightweight (~500 g) balloon-borne backscatter sonde developed at the Institute of Atmospheric and Climate Science, Swiss Federal Institute of Technology (ETH), Zurich. COBALD consists of two high-power (250 mW) light-emitting diodes (LEDs) that emit light at 455-nm (blue) and 940-nm (near-infrared) wavelengths. A silicon photodiode placed between the two LEDs collects the light backscattered from airborne particles (molecules, aerosols, and clouds). When connected to an iMet radiosonde, the instrument transmits backscatter counts at both of these wavelengths, pressure, temperature, relative humidity, wind speed, and wind direction at 1 Hz to the receiving ground station. The concurrent profiles of pressure, temperature, and backscattered counts are used to calculate scattering ratio (SR), the ratio of total backscattering coefficient ($\beta = \beta_p + \beta_m$) to the molecular backscattering coefficient β_m at a given wavelength. The ratio of ($SR_{940} - 1$) at 940 nm to ($SR_{455} - 1$) at 455 nm, defined as the color index (CI), gives qualitative information about particle size (Cirisan et al. 2014; Vernier et al. 2015).

MiniGAS. The miniGAS system is an integrated suite of instruments for unmanned aircraft vehicle (UAV) applications including meteorological (pressure, temperature) and up to five chemical sensors. The system uses a microcomputer, a datalogger, and a telemetry system from which gas concentrations can be displayed in real time on a laptop (Diaz et al. 2015). The miniGAS PRO version (Fig. 5) is designed for volcanic gas measurements on small UAVs, multicopter drones, and tethered balloons/blimps for <1.5 km AGL altitude flights. The miniGAS PRO was deployed during the 2018 VolKilau campaign for measuring SO_2 concentration from the Kilauea volcanic plume. The instrument collected SO_2 in the 0–20-ppm range and CO_2 in the 0–2,000-ppm range on two tethered flights coincident with OPC measurements. SO_2 and CO_2 measurements are based on electrochemical and nondispersive infrared techniques, respectively. A 0.2-μm polytetrafluoroethylene (PTFE) Teflon filter is included at the entrance of the sensor to limit the intrusion of droplets inside the miniGAS which might affect the measurements. However, we cannot completely rule out potential measurement artifacts at high relative humidity that may still affect in-cloud measurements.

Ozonesonde. Ozonesondes contain a payload that uses the ElectroChemical Cell (ECC) measurement technique to retrieve ozone concentration. Ozone reacts with potassium iodide following

$$2KI + O_3 + H_2O \rightarrow 2KOH + I_2 + O_2; \quad (1)$$

anode reaction:

$$3I- \rightarrow I_3^- + 2e^-; \quad (2)$$

cathode reaction (exposed to ambient air and the presence of O_3):

$$I_2 + 2e^- \rightarrow 2I^-. \quad (3)$$

SO_2 interferes with those measurements, however, and reacts with water following the reaction

$$SO_2 + 2H_2O \rightarrow 2e^- + SO_4^{2-} + 4H^+. \quad (4)$$

Each molecule of SO_2 produces two electrons, replenishing the cathode [Eq. (3)] and reducing the current between the anode and the cathode. The interference of SO_2 has been used to infer SO_2 information (Morris et al. 2010) using two sondes with and without an SO_2 filter. With the dual-sonde technique, SO_2 is inferred by subtracting the filtered signal (O_3) from the unfiltered signal ($O_3 + SO_2$). During the campaign, we attempted to use the dual-sonde technique but quickly realized that the levels of SO_2 were too high and led to the saturation of the signal. Thus, we used the ozonesonde only has an indicator to find the bottom of the volcanic plume

during the ascent and the top during the descent.

Impactor. Volcanic aerosol composition is investigated using an aerosol impactor, which was initially prepared for tethered balloon applications but only run on the ground because of weight limitations from Federal Aviation Administration (FAA) regulations and additional technical constraints. The MPS-3 Microanalysis Particle Sampler, a three-stage impactor, was connected to a small air pump delivering 1.4 L min^{-1} of flow. It was run for 30 min to sample 42 L of air. Inertial impaction sample collectors are associated with particle size cutoff diameters of 1.4 μm in stage 1 (S1) of the system, 0.2 μm in stage 2 (S2), and down to 0.05 μm in stage 3 (S3). After collection, the filters were placed in 2-mL sterile polypropylene vials with deionized water (resistivity: 18.2 Ω cm^{-1}) and extracted for three intervals of 10 min each, by ultrasonication at the Physical Research Laboratory, India. The subsequent solutions were analyzed by ion chromatography (DIONEX ICS 5000) to detect water-soluble cations (Na^+, NH_4^+, Mg^{2+}, K^+, Ca^{2+}) and anions (Cl^-, NO_3^-, SO_4^{2-}, NO^{2-}) using a cation column (DIONEX IonPac CS16) and anion column (DIONEX IonPac AS23), coupled to their respective suppressors CERS/AERS 500, before the conductivity detector (Thermoscientific P/N 061830; Patel and Rastogi 2018).

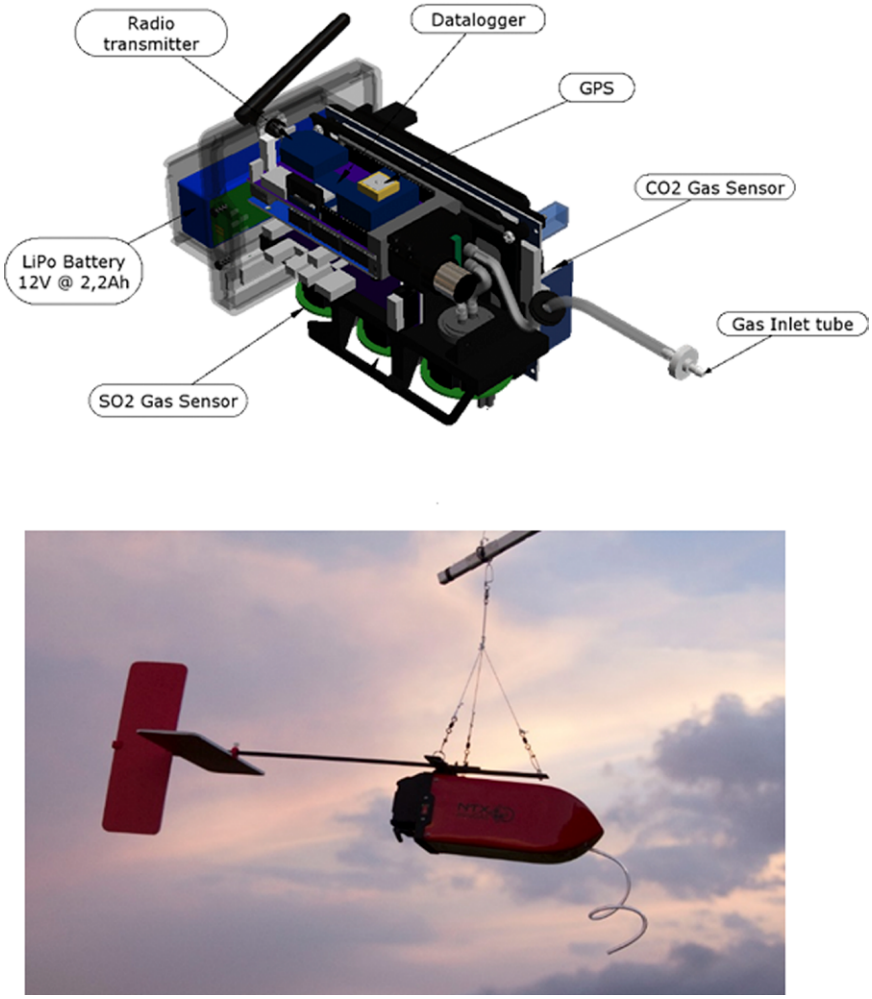

Fig. 5. (top) Schematic and (bottom) picture of the miniGAS PRO, a 1.5-kg miniature multiple-gas payload that incorporates waterproof case; GPS; and SO_2 and CO_2, temperature, and relative humidity sensors with onboard datalogger and telemetry, designed for UAV/drone or tethered-balloon/blimp measurements.

Balloon flights. The VolKilau campaign consisted of eight balloon flights between 11 and 18 June (Table 1) One flight took place from the Whittington Beach (19.086°N, 155.550°W) and the rest from the Kapapala Ranch (19.263°N, 155.445°W). We launched one low-level cut, four free-released, and four tethered flights during this time frame. The trajectories of the free-released balloon flights are shown in Fig. 6.

HYSPLIT trajectory model description. A custom version of the HYSPLIT model, referred to as the "vog model," was run in real time at the University of Hawai'i at Mānoa to produce forecasts of SO_2 and sulfate aerosol (Businger et al. 2015). The meteorological model input is a custom version of the Advanced Research version of the Weather Research and Forecasting Model (WRF-ARW) with 900-m horizontal resolution over the main Hawaiian Islands (Cherubini et al. 2008). For the Kilauea fissure eruptions, which did not produce explosive plumes that

Table 1. List of balloon flights during the VolKilau campaign together with date, time, location, flight type, payload, weight, and balloon size information. Impactor (G) is ground samples with the aerosol impactor, and (G, 12) is ground samples that were taken before VK01 on 12 Jun.

Date (UTC)	Location	Time (UTC)	Flight No.	Flight type	Maximum altitude	Payloads	Weight	Balloon
11 Jun	Kapapala	0400	Test	Tethered	100 m	ROPC	0.7 kg	300 g
13 Jun	Whittington Beach	0300	VK01	Free-released	28 km	LOPC, ECC, iMet, Impactor (12, G)	4.6 kg	1,200 g
14 Jun	Kapapala	0100	VK02	Free-released/ low-level cut	5 km	ROPC, miniGAS, Filter, Impactor (G)	2.0 kg	1,200 g
15 Jun	Kapapala	0600	VK03	Free-released	25 km	LOPC, COBALD, ECC	3.5 kg	1,200 g
15 Jun	Kapapala	2300	VK04	Tethered	1.2 km	ROPC, miniGAS	2.0 kg	300 g
16 Jun	Kapapala	2200	VK05	Tethered	1.1 km	LOPC, iMet	2.5 kg	1,200 g
16 Jun	Kapapala	2300	VK06	Free-released	25 km	iMet	0.2 kg	1,200 g
17 Jun	Kapapala	2200	VK07	Tethered	1.6 km	ROPC, miniGAS	1.2 kg	2,000 g
18 Jun	Kapapala	0100	VK08	Free-released	28 km	LOPC	2.6 kg	2,000 g

span the depth of the entire troposphere, the vog model did not have a release height scheme based on plume buoyancy but rather relied on correctly representing the mixed-layer depth. The vog forecasts were based on emission rates of SO_2 from the U.S. Geological Survey and Hawaiian Volcano Observatory. Prior to the LERZ eruptive event, the vog model incorporated real-time SO_2 emission estimates as weekly averages that were updated on a daily basis. These estimates were made using a UV spectrometer array (Elias et al. 2018) and acted as the primary source term for volcanic emissions in the vog model. The LERZ event interrupted operation of the UV spectrometer array. Less frequent estimates made with mobile instrumentation were used instead with differential optical absorption spectroscopy (DOAS) UV spectrometer. The frequency of updates had a direct and notable impact on vog model forecasts of concentrations (Holland et al. 2020). The model runs as shown in this study are based on the real-time operational system.

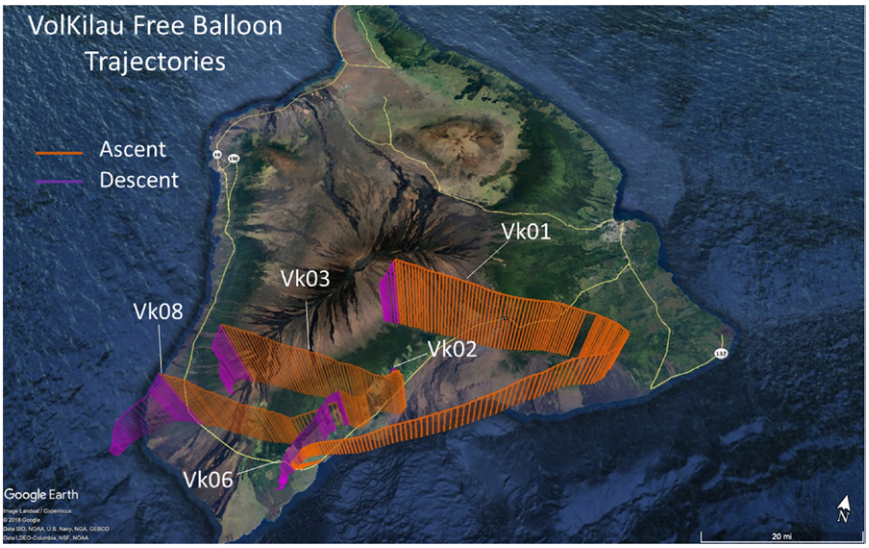

Fig. 6. Trajectories of the five free-released balloon flights during the VolKilau campaign. Balloon ascent is shown in orange and descent in magenta.

Campaign results

The VolKilau campaign dataset is analyzed together with satellite measurements of SO_2 and aerosols, and simulations using the HYSPLIT trajectory model.

Free-release flight into the Kilauea plume, VK01. After a tethered-balloon test flight on 11 June from the Kapapala Ranch, the first flight of the campaign (VK01) took place near 0300 UTC on 13 June with a combined flight of an OPC and an ECC for SO_2 information. Since SO_2 and wind forecasts showed that the volcanic plume was farther south than the Kapapala

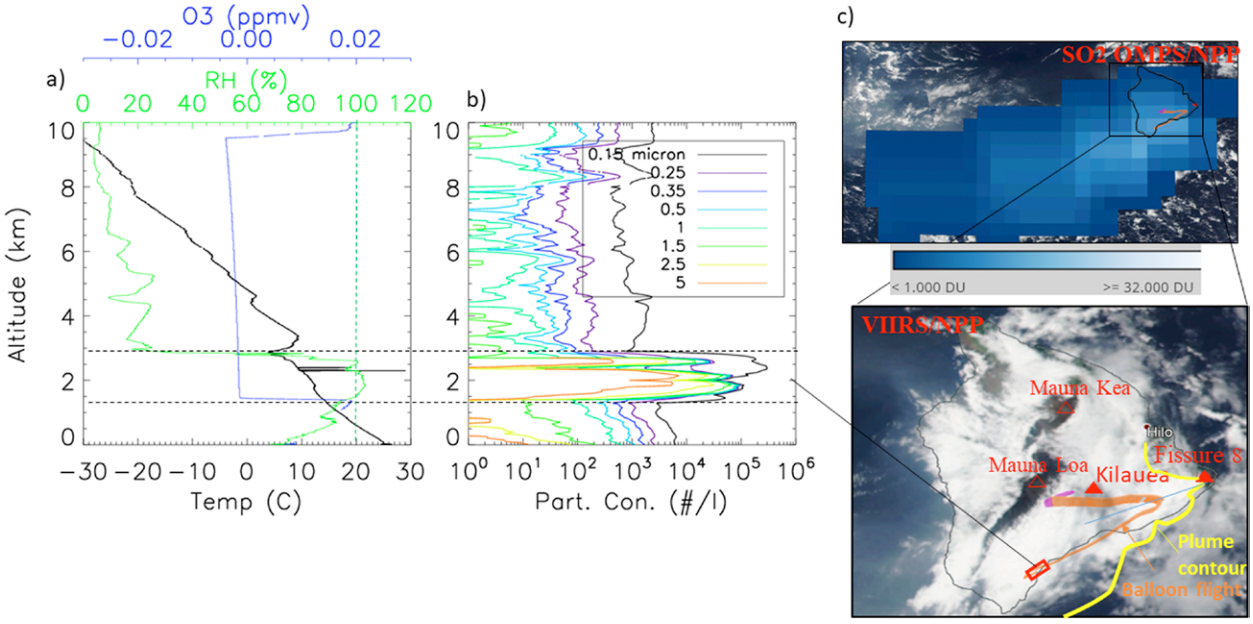

Fig. 7. Data from a free-released balloon flight (VK01) launched near 0300 UTC 13 Jun 2018 from Whittington Beach (19.086°N, 155.550°W). Profiles of (a) temperature, RH, and ozone mixing ratio and (b) aerosol concentration profiles for radius r > 0.15, 0.25, 0.35, 0.5, 1, 1.5, 2.5, and 5 μm. (c) Corresponding (top) SO_2 lower-tropospheric column map from OMPS/*SNPP* and (bottom) true-color image from VIIRS/*SNPP* near 2300 UTC 12 Jun superimposed with balloon flight trajectory. Volcanic plume emitted from Fissure 8 in the LERZ is drawn with a yellow contour.

Ranch, we decided to move our equipment along the shore of Hawaii near Whittington Beach (19.086°N, 155.549°W). Figure 7 shows aerosol concentration profiles for r > 0.15, 0.25, 0.35, 0.5, 0 1, 1.5, 2.5, and 5 μm associated with relative humidity (RH) and temperature profiles. A corresponding VIIRS true-color image and an SO_2 lower-tropospheric column map from the OMPS instrument 3–4 h before the balloon flight are also shown. The SO_2 cloud is seen over Hawaii, extending farther south-southwest across the Pacific Ocean. The true-color image shows a white cloud (delineated by yellow contours) originating from Fissure 8. The ozone profile is shown to decrease rapidly from 0.02 ppmv to negative values near 1.3 km aloft due to the presence of SO_2, consistent with the base of the volcanic plume. Due to saturation effects from large concentrations of SO_2 in the ECC cell, the signal remained below 0 during the ascent even though the sonde was already out of the plume as indicated by the OPC data. Near 1.3 km, the aerosol concentration for r > 0.15 μm increases by a factor of 10 within a few hundred meters, also indicating the base of the volcanic plume. Volcanic aerosols are especially enhanced for the largest sizes when RH > 100% as observed between 1.5 and 2.2 km, suggesting that saturated conditions favor the formation and growth of large sulfate aerosols. The volcanic cloud is observed between 1.5 and 3.5 km (MSL) altitude with a maximum of number concentration for r > 0.15 μm near 2.5 km with values reaching 3×10^5 L^{-1} where the RH is below 100%. Above saturation, aerosol concentration of r > 5 μm peaks near 1×10^4 L^{-1} (near 2.2 km), nearly four orders of magnitude larger than at 2.5 km. The wind direction (40°–60°) traces back the 1.5–3.5-km layer to volcanic emissions from Fissure 8, 80 km away, and the wind speed (10–11 m s^{-1}) indicates a plume age of ~2.2 h. Relative variations of aerosol concentration in function of RH reveal potential interaction between volcanic aerosols and water clouds. Saturated levels seem to favor the growth and dissolution of sulfate aerosols in liquid water clouds with large sulfuric acid droplets while subsaturated conditions generate smaller particles likely through new particle formation (Rose et al. 2019; Boulon et al. 2011) from photooxidation and the growth of sulfate aerosols from SO_2.

High-resolution OPC data, VK02. We conducted a low-level balloon flight (<5 km) using a radio-controlled cut-down system to sample the plume and terminate the flight to optimize the chance to recover the payloads. This balloon flight was launched near 0100 UTC on 14 June (VK02) from the Kapapala Ranch downwind from volcanic emissions of Fissure 8 (Fig. 8) and nearly 2 h after an overpass of the Moderate Resolution Imaging Spectroradiometer (MODIS) on the *Aqua* satellite. The flight was terminated at 5-km height but, despite the accurate location of the landing, we could not recover the payloads. The ascent and descent profiles (Fig. 8) show high concentration of aerosols up to 3 km like the previous day with the presence of larger aerosols within the cloud. The volcanic plume is capped by a trade wind inversion at 2.9 km with dry air from the free troposphere above this level. Wind speed within the layer between 4 and 9 m s^{-1} from 0° to 70°N is consistent with its origin from Fissure 8, 2–4 h prior to our measurements. While the optical particle counter was at the coincidence counting limit throughout the plume (3×10^5 L^{-1}) from 1.2 to 2.9 km, the measurements qualitatively show significant structure within the plume with a series of ~100-m-thick layers from 1.9 to 2.5 km on ascent with significantly varying aerosol size distributions. After the flight was remotely terminated, the instrument descended through the volcanic plume, reentering the

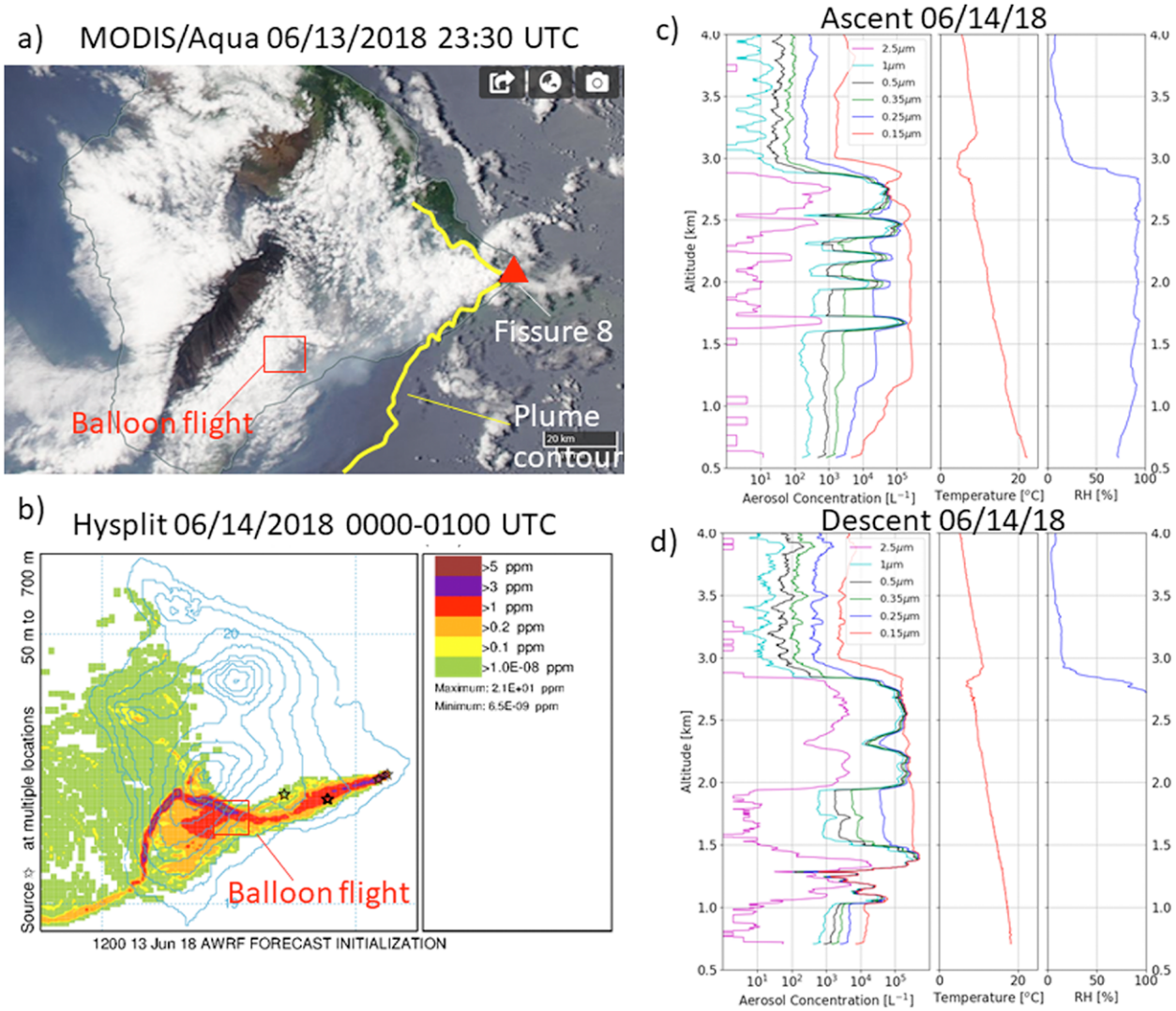

Fig. 8. (a) True-color image from MODIS on the *Aqua* satellite near 2330 UTC 13 Jun and (b) SO_2 mixing ratio derived from HYSPLIT between 0000 and 0100 UTC 14 Jun. (c),(d) Temperature, RH, and aerosol concentration profiles for sizes ranging from 0.15 to 5 μm during the ascent and descent, respectively, of the balloon flight (VK02) launched from the Kapapala Ranch (19.263°N, 155.445°W) near 0100 UTC 14 Jun.

plume approximately 2 km north of the ascent profile. This descent profile shows a similar overall vertical extent to the plume, but the structure within the plume is significantly different. Throughout the descent the RH in the plume was greater than 100%, probably causing the majority of the aerosol to grow to radii above 1 μm, and reducing the vertical structure within the plume. The descent took place in a cloudy area as observed by MODIS (Fig. 8), confirming the presence of large water droplets as observed by the OPC. During the descent and below 2.5 km, RH is blocked at 104%, which may suggest instrument hysteresis issues in cloud interstitial conditions. Both the internal structure observed during ascent profile and the differences between the relatively closely spaced ascent and descent profiles reinforce the importance of considering inhomogeneity within the plume as well as cloud–aerosol interactions.

Satellite comparison, VK03. One of the objectives of the VolKilau campaign was to compare and validate satellite observations using our balloon data. A nearly coincident balloon flight was planned at 0600 UTC on 15 June with a nearby overpass of the *CALIPSO* satellite (within 200 km and 6 h) downwind from Fissure 8 and our balloon measurements. The measurements included an ECC, a backscatter sonde (COBALD), and the LOPC shown in Fig. 9. The ECC saturated (not shown) because of high concentration of SO_2 (horizontal line near 1.2 km, Fig. 9b), thus the unfiltered ECC data went to zero coincidently with an increase of aerosol concentration. A second aerosol layer is observed near 4–4.5 km on both aerosol instruments consistent with the volcanic plume. Both layers are correlated with increasing RH between 40% and 95%, consistent with expected aerosol growth in humid environment as observed near the Etna volcano (Roberts et al. 2018). Those moist layers very likely originate from Fissure 8

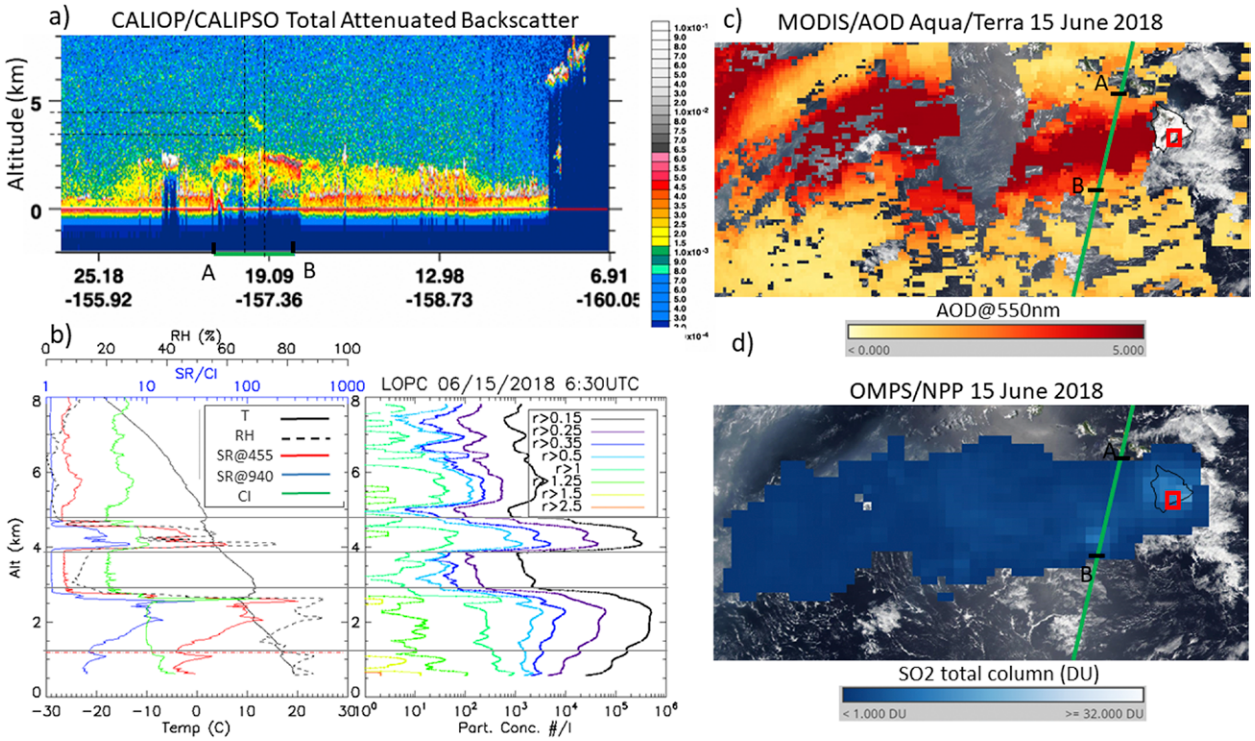

Fig. 9. (a) Total attenuated backscatter from CALIOP/*CALIPSO* at 1200 UTC 15 Jun. (b) Temperature (*T*), RH, aerosol concentration profiles from the LOPC and scattering ratios (SR@455 nm, SR@940), and color index (CI = SR@940/SR@455) from the COBALD backscatter sonde launched near 0600 UTC 15 Jun (VK03). (c) MODIS AOD from *Aqua/Terra* and (d) SO_2 lower-tropospheric column from OMPS/*SNPP* with the *CALIPSO* orbit track position shown in green. OMPS and MODIS have been obtained from https://worldview.earthdata.nasa.gov/.

with wind speed near 3–7 m s^{-1} coming from the 0°–60°N direction, yielding a plume age near 2–5 h. The *CALIPSO* overpass 200 km downwind and 6 h after the flight, also indicate a double layer, one in the boundary layer capping at 3 km and another in the free troposphere near 4 km. SO_2 and Aerosol Optical Depth (AOD) maps from OMPS/*SNPP* and MODIS/*Terra*/*Aqua* also indicate the dispersion of the volcanic cloud westward downwind from Fissure 8, across the western Pacific. *CALIPSO* intersected the volcanic plume associated with high SO_2 and AOD from MODIS and OMPS and is coincident with high backscatter values and low depolarization (not shown) consistent with the presence of liquid sulfate aerosols for both layers. Wind speed and direction near 4-km height observed on the balloon flight (6 m s^{-1}, 50–60°) are consistent with the movement of air masses moving south-southeast and crossing the *CALIPSO* overpass after 6 h. Those measurements indicate that volcanic materials from Fissure 8 had a complex vertical and horizontal distribution depending on weather conditions and atmospheric instability. Reports from the National Weather Service (https://twitter.com/nwshonolulu/status/1013890724448866305) indicated convective cloud induced by heat from Fissure 8 that could have transported volcanic materials at high altitudes. However, no trace of volcanic aerosols above 5 km was observed by satellites or during the VolKilau campaign. Nevertheless, those observations indicate that parts of the Kilauea volcanic plume were transported in the free troposphere above the boundary layer.

Volcanic plume chemical and microphysical changes, VK04. Volcanic plume chemistry is investigated by combining temperature, RH, aerosols, SO_2, and CO_2/SO_2 using a tethered-balloon flight on 15 June 2018 from the Kapapala Ranch (VK04). The time series of those parameters between 2316 and 2345 UTC is shown in Figs. 10a–c together with geolocation of the balloon flight on Google Maps colored with SO_2 measurements (Fig. 10e). Levels of SO_2

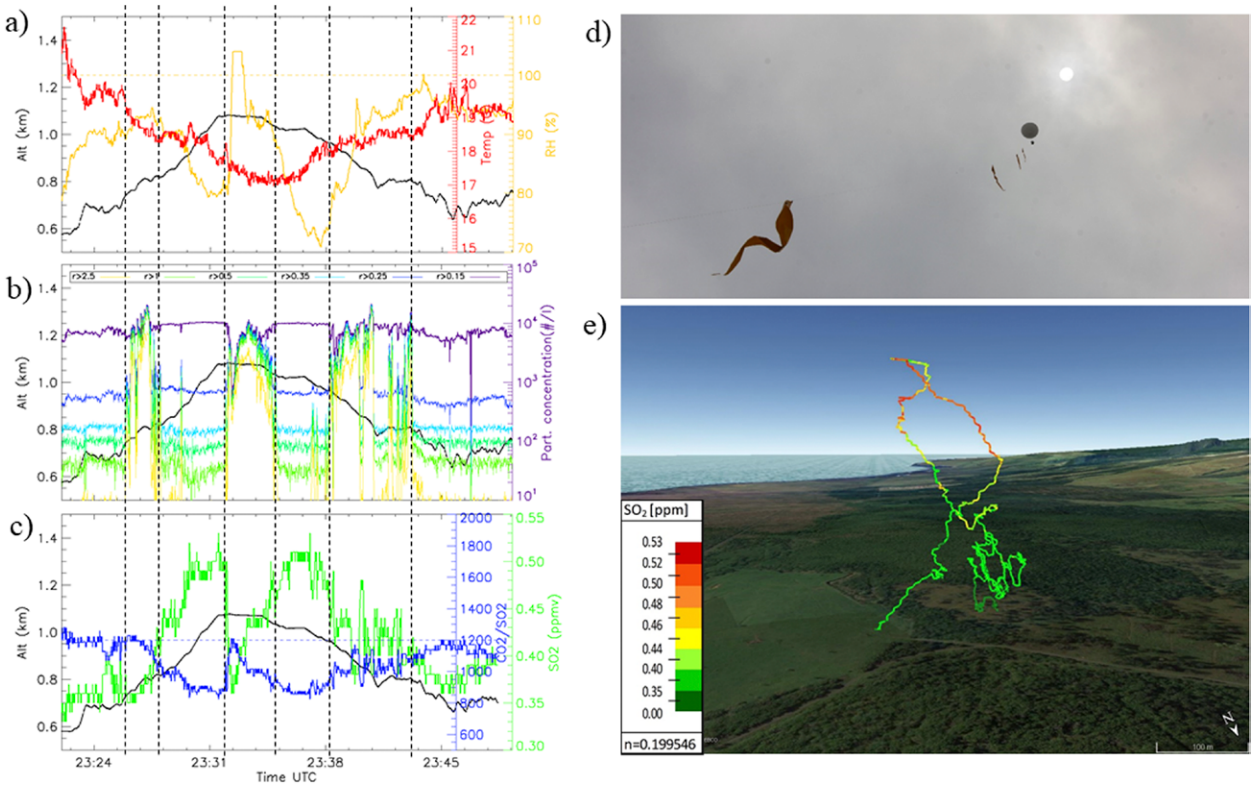

Fig. 10. (left) Time series of (a) temperature and RH, (b) aerosol concentration, and (c) SO_2 mixing ratio and CO_2/SO_2 ratio between 2320 and 2350 UTC on 15 Jun using GPS-measured altitudes. Aerosol and SO_2 concentrations were measured by the ROPC and miniGAS, respectively. (right) Photoraphs of (d) upward-looking view of the tethered system and (e) balloon position colored with SO_2 mixing ratio on Google Maps.

near the surface were approaching 0.3 ppmv and increased up to 0.5 ppmv at 2331 UTC just before entering a water cloud near 1 km MSL, as indicated by RH near 100% and a sudden increase of particle concentrations for sizes between 0.5 and 10 μm. The tethered balloon was brought down from the clouds to ensure FAA compliance which requires continuous in-operation line-of-sight view on the system. Outside the water cloud, the RH dropped to 70% and SO_2 levels regained their levels near 0.5 ppmv while the concentration of aerosols dropped. CO_2 concentration was nearly constant within the plume so that the increase of the CO_2/SO_2 ratio observed in Fig. 10 was driven by the sharp drop of SO_2 and likely suggests the absence of SO_2 within clouds. However, we cannot exclude that cloud droplets affected the miniGAS measurements despite the presence of a PTFE filter at the entrance to prevent the intrusion of sulfuric acid droplets. Coincident measurements of SO_2 and aerosols near the vent of volcano likely reveal the interaction between water vapor, SO_2, and aerosols (Roberts et al. 2018). In-cloud SO_2 decreased rapidly probably because of different aqueous pathways leading to the formation of sulfate either from the oxidation of H_2O_2 (Carn et al. 2011), O_3, and/or the TMI-O2 pathway (Galeazzo et al. 2018) even if we cannot rule out potential measurement artifacts of SO_2 in high RH conditions.

Volcanic aerosol composition. Volcanic composition is investigated using an aerosol impactor. We show the ionic composition of two samples, HS1 (Hawaii sample 1) and HS2 (Hawaii sample 2) collected at 0530 UTC 12 June and 0744 UTC 14 June 2018, respectively, for 30 min each, with a flow of 1.4 L min^{-1} for a total of 42 L of air sampled. Stages 1 and 2 for the two sets of samples hold similar concentrations of major ions in aerosols between 3,950 and 5,900 ng m^{-3}. Here, Na^+ and Cl^- ions dominate the total ionic mass with a smaller contribution of SO_4^{2-} in stage 1 ($r > 1.4$ μm) and stage 2 (1.4 μm $< r <$ 0.05 μm). The major difference observed between the two samples is in stage 3 ($r \leq 0.05$ μm), where the concentration of SO_4^{2-} and NH_4^+ aerosols are 6.2 and 7.9 times higher, respectively, in HS2 compared to HS1 (Fig. 11). Those

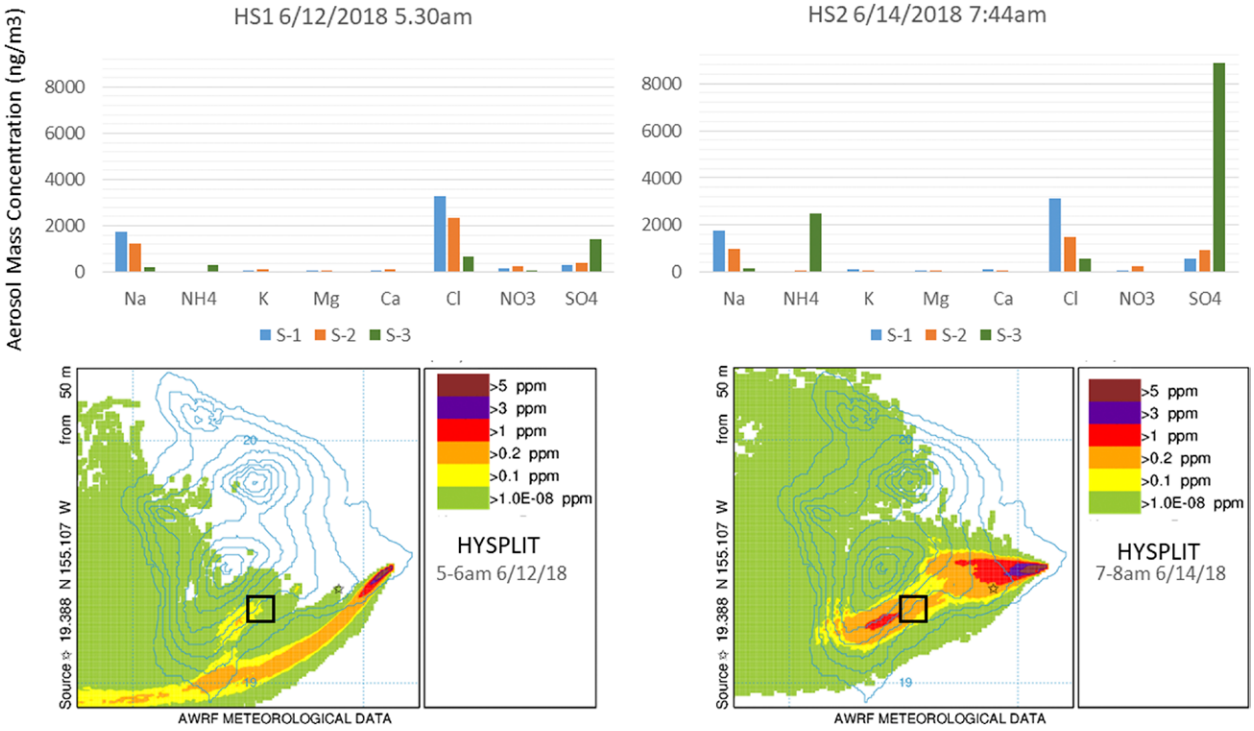

Fig. 11. (top) Ionic concentrations from aerosol samples collected at (left) 0530 UTC 12 Jun (HS1) and (right) 0744 UTC 14 Jun (HS2). (bottom) SO_2 mixing ratio between 0 and 100 m from HYSPLIT near the time of the sampling.

Table 2. Ionic concentration (ng m^{-3}) for the two ground aerosol samples taken during the VolKilau campaign at 0530 UTC 12 Jun 2018 (HS1) and 0744 UTC 14 Jun 2018 (HS2).

	Na^+	NH^{4+}	K^+	Mg^{2+}	Ca^{2+}	Cl^-	NO_2^-	NO_3^-	SO_4^{2-}
0530 UTC 12 Jun 2018 (HS1)									
S1	1,747	0	0	0	0	3,300	0	159	327
S2	1,249	0	145	0	144	2,364	0	245	418
S3	204	307	0	0	0	674	0	0	1,429
0744 UTC 14 Jun 2018 (HS2)									
S1	1,759	0	122	0	122	3,151	0	0	599
S2	991	0	0	0	0	1,474	0	263	928
S3	182	2,466	0	0	0	577	0	0	8,862

measurements are compared with HYSPLIT simulations at the time of the collections. HYSPLIT also shows a much larger concentration of SO_2 (by a factor of 2–10) during HS2 compared to HS1, consistent with favorable meteorological conditions bringing volcanic material toward the measurement on 14 June compared to 12 June, when trade winds pushed volcanic aerosols offshore (Table 2). Further, Cl^-/Na^+ ratios in stages 1 and 2 of samples HS1 and HS2 were similar to their sea salt ratio (1.8); however, in stage 3 the ratio was about 3.3, that is, ~2 times higher than expected from sea salt. This observation suggests the presence of excess Cl^- in stage 3 in both the samples. Relatively high Cl^- in stage 3 likely indicates a significant contribution of Cl^- from volcanic emissions themselves and/or resulting from the hydrochloric acid emissions from lava entering the ocean (Resing and Sansone 1999). Furthermore, the non–sea salt (nss) fraction of SO_4^{2-}, estimated using the SO_4^{2-}/Na^+ ratio in sea salt as a reference, was low in stages 1 and 2 but close to 100% in stage 3. We note also the presence of NH_4^+ in stage 3 of HS1 and HS2, bearing somewhat similar relative concentration with nss SO_4^{2-}, indicating the presence of SO_4^{2-} aerosol in the form of $(NH_4)_2SO_4$. While the presence of SO_4^{2-} is consistent with the rapid conversion of SO_2 into sulfate aerosols in the troposphere, its apparent association with NH_4^+ is interesting. The neutralization of acidic volcanic sulfate by ammonia has already been observed after the 2011 Grímsvötn volcano 3,000 km from the sources. This process is size dependent with the neutralization efficiency enhanced for small particles (Šakalys et al. 2016). Our results also suggest that the neutralization of sulfate near the ground was dominant for particles smaller than 50-nm diameter. However, the level of neutralization was much larger than those found by Kroll et al. (2015), who reported a ratio of SO_4^{2-}/NH_4^+ between 10 and 20 at Pahala less than 10 km away from our measurement site. The proximity of livestock could explain the increased neutralization levels of sulfate with ammonium. However, a significant fraction of SO_4^{2-} was present as free acid as indicated by observed mass ratio of sulfate/ammonium (3.6) in comparison to expected mass ratio (2.7) if all sulfate would have existed as $(NH_4)_2SO_4$.

Conclusions

The 2018 Kilauea eruption was the most significant volcanic event in the United States since Mount Saint Helens erupted almost four decades ago. Our team deployed quickly in Hawaii to (i) obtain vertically resolved profiles of SO_2, aerosol, and meteorological parameters; (ii) validate satellite observations; and (iii) be better prepared for the next large volcanic eruption. We deployed to Hawaii within 15 days between 11 and 18 June 2018 with eight flights of tethered, low-level cut, and free-released balloon activities from a ranch downwind from active volcanic fissures and the Kilauea main crater. We flew multiple times in the volcanic plume from Fissure 8 emissions and found aerosol number concentration up to $3 \times 10^5\ L^{-1}$. Coincident measurements between SO_2, aerosol concentration, and RH suggest rapid conversion of SO_2

into aerosols in supersaturated conditions leading to the formation of vog. Satellite observations and balloon data demonstrate the complexity of volcanic emissions with multiple volcanic layers observed up to 4.5–5 km MSL in the free troposphere. Finally, chemical analysis of ground-based samples shows the recurrent presence of sea salt (NaCl) together with volcanic sulfate. The mass concentration of sulfate was shown to vary by as much as a factor of 6 within a few days depending on wind conditions, as revealed by HYSPLIT simulations and our measurements. An excess of Cl^- relative to the Cl^-/Na^+ ratio of sea salt revealed sources from the magma itself and/or the influence of hydrochloric acid emissions from lava entering the ocean (Resing and Sansone 1999). The presence of ammonium in the samples suggests that acidic volcanic sulfate is rapidly neutralized by the ammonia released by livestock, which were in proximity to the measurement location. The VolKilau mission represented a unique opportunity to combine SO_2 and aerosol measurements to understand aerosol microphysics in the Kilauea volcanic plume. Looking forward, we have successfully tested our instruments in the tropospheric volcanic plume environment so that they can be used during future large volcanic eruptions.

Acknowledgments. This work was supported through the NASA Earth Science UARP and Disasters programs by K. Jucks, J. Kaye, and D. Green at NASA HQ. We thank the owners of the Kapapala Ranch for using their property during the field mission. We thank Tara for using her lab at the UH-Hilo Analytical Laboratory. We thank D. Pieri from JPL for putting us in touch with Kapapala Ranch owner. We thank Jason from EPA for helping us get access to the restricted area in Leilani Estates. We thank Timothy Edward for preparing Fig. 4. The MODIS, VIIRS, and OMPS maps were obtained from https://worldview.earthdata.nasa.gov/.

References

Boulon, J., K. Sellegri, M. Hervo, and P. Laj, 2011: Observations of nucleation of new particles in a volcanic plume. *Proc. Natl. Acad. Sci. USA,* **108,** 12 223–12 226, https://doi.org/10.1073/pnas.1104923108.

Businger, S., R. Huff, K. Horton, A. J. Sutton, and T. Elias, 2015: Observing and forecasting vog dispersion from Kīlauea Volcano, Hawaii. *Bull. Amer. Meteor. Soc.*, **96**, 1667–1686, https://doi.org/10.1175/BAMS-D-14-00150.1.

Carn, S. A., and Coauthors, 2011: In situ measurements of tropospheric volcanic plumes in Ecuador and Colombia during TC4. *Geophys. Res. Lett.*, **116**, D00J24, https://doi.org/10.1029/2010JD014718.

Cherubini, T., S. Businger, R. Lyman, and M. Chun, 2008: Modeling optical turbulence and seeing over Mauna Kea. *J. Appl. Meteor. Climatol.*, **47**, 1140–1155, https://doi.org/10.1175/2007JAMC1487.1.

Cirisan, A., and Coauthors, 2014: Balloon-borne match measurements of midlatitude cirrus clouds. *Atmos. Chem. Phys.*, **14**, 7341–7365, https://doi.org/10.5194/acp-14-7341-2014.

Diaz, J. A., and Coauthors, 2015: Unmanned aerial mass spectrometer systems for in-situ volcanic plume analysis. *J. Amer. Soc. Mass Spectrom.*, **26**, 292–304, https://doi.org/10.1007/s13361-014-1058-x.

Draxler, R., and G. D. Hess, 1997: Description of the HYSPLIT_4 modelling system. NOAA Tech. Memo. ERL ARL-224, 27 pp., www.arl.noaa.gov/documents/reports/arl-224.pdf.

Elias, T., C. Kern, K. Horton, A. Sutton, and H. Garbeil, 2018: Measuring SO_2 emission rates at Kīlauea Volcano, Hawaii, using an array of upward-looking UV spectrometers, 2014–2017. *Front. Earth Sci.*, **6**, 214, https://doi.org/10.3389/feart.2018.00214.

Flynn, L., and Coauthors, 2014: Performance of the Ozone Mapping and Profiler Suite (OMPS) products. *J. Geophys. Res. Atmos.*, **119**, 6181–6195, https://doi.org/10.1002/2013JD020467.

Galeazzo, T., S. Bekki, E. Martin, J. Savarino, and S. R. Arnold, 2018: Photochemical box modelling of volcanic SO_2 oxidation: Isotopic constraints. *Atmos. Chem. Phys.*, **18**, 17 909–17 931, https://doi.org/10.5194/acp-18-17909-2018.

Grattan, J., M. Durand, and S. Taylor, 2003: Illness and elevated human mortality in Europe coincident with the Laki Fissure eruption. *Geol. Soc. London Spec. Publ.*, **213**, 401–414, https://doi.org/10.1144/GSL.SP.2003.213.01.24.

Hansell, A., and C. Oppenheimer, 2004: Health hazards from volcanic gases: A systematic literature review. *Arch. Environ. Health*, **59**, 628–639, https://doi.org/10.1080/00039890409602947.

——, C. Horwell, and C. Oppenheimer, 2006: The health hazards of volcanoes and geothermal areas. *Occup. Environ. Med.*, **63**, 149–156, https://doi.org/10.1136/oem.2005.022459.

Holland, L., S. Businger, T. Elias, and T. Cherubini, 2020: Two ensemble approaches for forecasting sulfur dioxide emissions from Kīlauea Volcano. *Wea. Forecasting*, https://doi.org/10.1175/WAF-D-19-0189.1, in press.

Ialongo, I., and Coauthors, 2015: Comparison of operational satellite SO_2 products with ground-based observations in northern Finland during the Icelandic Holuhraun fissure eruption. *Atmos. Meas. Tech.*, **8**, 2279–2289, https://doi.org/10.5194/amt-8-2279-2015.

Kroll, J. H., and Coauthors, 2015: Atmospheric evolution of sulfur emissions from Kīlauea: Real-time measurements of oxidation, dilution, and neutralization within a volcanic plume. *Environ. Sci. Technol.*, **49**, 4129–4137, https://doi.org/10.1021/es506119x.

Li, C., N. A. Krotkov, Y. Zhang, P. Leonard, J. Joiner, 2017: OMPS/NPP PCA SO_2 total column 1-orbit L2 Swath 50 × 50km V1. Goddard Earth Sciences Data and Information Services Center (GES DISC), accessed 15 June 2019, https://doi.org/10.5067/MEASURES/SO2/DATA203.

Longo, B. M., 2013: Adverse health effects associated with increased activity at Kīlauea Volcano: A repeated population-based survey. *ISRN Public Health*, **2013**, 1–10, https://doi.org/10.1155/2013/475962.

Mather, T. A., A. G. Allen, C. Oppenheimer, D. M. Pyle, and A. J. S. McGonigle, 2003: Size-resolved characterisation of soluble ions in the particles in the tropospheric plume of Masaya volcano, Nicaragua: Origins and plume processing. *J. Atmos. Chem.*, **46**, 207–237, https://doi.org/10.1023/A:1026327502060.

——, and Coauthors, 2012: Halogens and trace metal emissions from the ongoing 2008 summit eruption of Kīlauea volcano, Hawai'i. *Geochim. Cosmochim. Acta,* **83,** 292–323, https://doi.org/10.1016/j.gca.2011.11.029.

McCormick, M. P., L. W. Thomason, and C. R. Trepte, 1995: Atmospheric effects of the Mt Pinatubo eruption. *Nature*, **373**, 399–404, https://doi.org/10.1038/373399a0.

Morris, G. A., W. D. Komhyr, J. Hirokawa, J. Flynn, B. Lefer, N. Krotkov, and F. Ngan, 2010: A balloon sounding technique for measuring SO_2 plumes. *J. Atmos. Oceanic Technol.*, **27**, 1318–1330, https://doi.org/10.1175/2010JTECHA1436.1.

Neal, C. A., and Coauthors, 2019: The 2018 rift eruption and summit collapse of Kilauea Volcano. *Science*, **363**, 367–374, https://doi.org/10.1126/science.aav7046.

Patel, A., and N. Rastogi, 2018: Oxidative potential of ambient fine aerosol over a semiurban site in the Indo-Gangetic Plain. *Atmos. Environ.*, **175**, 127–134, https://doi.org/10.1016/j.atmosenv.2017.12.004.

Pieri, D., and Coauthors, 2013: In situ observations and sampling of volcanic emissions with NASA and UCR unmanned aircraft, including a case study at Turrialba Volcano, Costa Rica. *Geol. Soc. London Spec. Publ.,* **380,** 321–352, https://doi.org/10.1144/SP380.13.

Resing, J. A., and F. J. Sansone, 1999: The chemistry of lava–seawater interactions: The generation of acidity. *Geochim. Cosmochim. Acta*, **63**, 2183–2198, https://doi.org/10.1016/S0016-7037(99)00193-3.

Roberts, T., G. Dayma, and C. Oppenheimer, 2019: Reaction rates control high-temperature chemistry of volcanic gases in air. *Front. Earth Sci.*, **7**, 154, https://doi.org/10.3389/feart.2019.00154.

——, and Coauthors, 2018: The primary volcanic aerosol emission from Mt Etna: Size-resolved particles with SO_2 and role in plume reactive halogen chemistry. *Geochim. Cosmochim. Acta*, **222**, 74–93, https://doi.org/10.1016/j.gca.2017.09.040.

Robock, A., 2000: Volcanic eruptions and climate. *Rev. Geophys.*, **38**, 191–219, https://doi.org/10.1029/1998RG000054.

Rose, C., B. Foucart, D. Picard, A. Colomb, J.-M. Metzger, P. Tulet, and K. Sellegri, 2019: New particle formation in the volcanic eruption plume of the Piton de la Fournaise: Specific features from a long-term dataset. *Atmos. Chem. Phys.,* **19**, 13 243–13 265, https://doi.org/10.5194/acp-19-13243-2019.

Sahyoun, M., and Coauthors, 2019: Evidence of new particle formation within etna and stromboli volcanic plumes and its parameterization from airborne in situ measurements. *J. Geophys. Res. Atmos.*, **124**, 5650–5668, https://doi.org/10.1029/2018JD028882.

Šakalys, J., E. Meinorė, and K. Kvietkus, 2016: Neutralization of acidic sulfates with ammonia in volcanic origin aerosol particles. *Lith. J. Phys.*, **56**, 42–48, https://doi.org/10.3952/physics.v56i1.3275.

Seftor, C. J., G. Jaross, M. Kowitt, M. Haken, J. Li, and L. E. Flynn, 2014: Postlaunch performance of the Suomi national polar-orbiting partnership Ozone Mapping and Profiler Suite (OMPS) nadir sensors. *J. Geophys. Res. Atmos.*, **119**, 4413–4428, https://doi.org/10.1002/2013JD020472.

Small, C., and T. Naumann, 2001: The global distribution of human population and recent volcanism. *Global Environ. Change,* **3B**, 93–109, https://doi.org/10.1016/S1464-2867(02)00002-5.

Stein, A. F., R. R. Draxler, G. D. Rolph, B. J. B. Stunder, M. D. Cohen, and F. Ngan, 2015: NOAA's HYSPLIT atmospheric transport and dispersion modeling system. *Bull. Amer. Meteor. Soc.*, **96**, 2059–2077, https://doi.org/10.1175/BAMS-D-14-00110.1.

Surl, L., D. Donohoue, A. Aiuppa, N. Bobrowski, and R. Von Glasow, 2015: Quantification of the depletion of ozone in the plume of Mount Etna. *Atmos. Chem. Phys.*, **15**, 2613–2628, https://doi.org/10.5194/acp-15-2613-2015.

Vernier, J.-P., and Coauthors, 2015: Increase in upper tropospheric and lower stratospheric aerosol levels and its potential connection with Asian pollution. *J. Geophys. Res. Atmos.*, **120**, 1608–1619, https://doi.org/10.1002/2014JD022372.

——, and Coauthors, 2018: BATAL: The balloon measurement campaigns of the Asian tropopause aerosol layer. *Bull. Amer. Meteor. Soc.*, **99**, 955–973, https://doi.org/10.1175/BAMS-D-17-0014.1.

Vignelles, D., and Coauthors, 2016: Balloon-borne measurement of the aerosol size distribution from an Icelandic flood basalt eruption. *Earth Planet. Sci. Lett.*, **453,** 252–259, https://doi.org/10.1016/j.epsl.2016.08.027.

Witham, C., and C. Oppenheimer, 2004: Mortality in England during the 1783-4 Laki craters eruption. *Bull. Volcanol.*, **67**, 15–26, https://doi.org/10.1007/s00445-004-0357-7.

Zhang, Y., C. Li, N. A. Krotkov, J. Joiner, V. Fioletov, and C. McLinden, 2017: Continuation of long-term global SO_2 pollution monitoring from OMI to OMPS. *Atmos. Meas. Tech.*, **10**, 1495–1509, https://doi.org/10.5194/amt-10-1495-2017.